


Flow Resistance in Very Rough Channels

Journal Article**Author(s):**

Deal, Eric 

Publication date:

2022-10

Permanent link:

<https://doi.org/10.3929/ethz-b-000579633>

Rights / license:

[Creative Commons Attribution-NonCommercial 4.0 International](#)

Originally published in:

Water Resources Research 58(10), <https://doi.org/10.1029/2021WR031790>

Water Resources Research®

RESEARCH ARTICLE

10.1029/2021WR031790

Flow Resistance in Very Rough Channels

E. Deal¹ 

¹Department of Earth Sciences, ETH Zürich, Zürich, Switzerland

Key Points:

- A semiempirical model of form drag on boulders is shown to be consistent with flow resistance in rough channels
- Data are suggestive that geometry and flow resistance in rough channels are conditioned to maximize flow resistance, leading to convergence in behavior

Correspondence to:

E. Deal,
eric.deal@erdw.ethz.ch

Citation:

Deal, E. (2022). Flow resistance in very rough channels. *Water Resources Research*, 58, e2021WR031790. <https://doi.org/10.1029/2021WR031790>

Received 8 DEC 2021
Accepted 11 SEP 2022

Abstract Flow resistance in open channels determines the average flow velocity in a river, with important implications for downstream and at-a-station hydraulic geometry and sediment transport in natural channels. However, flow resistance in steep mountain channels is challenging to understand and predict due to heterogeneous channel morphology and spatially variable flow. Using a double-averaging approach appropriate for very rough channels, the width, reach, and double-averaged variables for steady, uniform flow in an open channel are derived. Using an empirical model for the coefficient of form drag, a flow resistance model is derived that compares well to a large data set of flow velocity in natural channels. Several parameters that together describe bed morphology are observed to be relatively consistent in the data set used and compare well to previous estimates of their values. This implies a degree of self-organization in bed morphology that may simplify the challenging problem of predicting flow resistance in steep mountain rivers.

1. Introduction

Flow resistance in open channels, that is, the friction that the channel boundary exerts on the flow, is a fundamental hydraulic parameter defining many aspects of the behavior of a river channel (Kalathil & Chandra, 2019; Powell, 2014; Shobe et al., 2021). The roughness of the channel boundary relative to the depth of the flow is one of the primary influences on flow resistance (Cheng, 2017; Ferguson, 2007; Nitsche et al., 2012; Powell, 2014), and river channels can be broadly divided into two categories based on boundary roughness.

The first category are those channels where the flow is significantly deeper than the scale of the boundary roughness, for example, deep relative to the characteristic grain size or bedform height. In these flows, the fluid momentum is dissipated in a roughness boundary layer that is thin relative to the full flow depth. The small scale of the roughness boundary layer relative to the depth of the flow ensures that the spatial variability in flow resistance is low, allowing the flow to reasonably be treated as steady and uniform. Overall, the effect of the boundary layer on the flow is well captured by a simple adjustment to the log law of the wall depth-velocity profile based on a roughness length-scale. Although the details of how any particular boundary configuration gives rise to a particular roughness length-scale are still poorly understood (Brereton et al., 2021; Chung et al., 2021), a length-scale of $\sim 3D_{84}$ is commonly used for natural channels (Bathurst, 1985; Lamb et al., 2017a). The D_{84} is the grain diameter larger than 84% of the grains on a bed, and is commonly used to characterize the grain sizes in a river channel.

This is in contrast to the second category where the boundary roughness length-scale is as large or larger than the flow depth due to roughness elements such as immobile boulders, often found in steep mountain environments. The flow resistance for these channels is high and generally underpredicted by models developed for relatively smooth boundaries (Kalathil & Chandra, 2019; Powell, 2014; Shobe et al., 2021). Because the roughness boundary layer occupies much or all of the flow depth, the poor understanding of flow within this layer becomes especially problematic. In addition, the flow resistance tends to be spatially variable, varying from one channel cross-section to another, and the flow is unlikely to be steady or uniform. Despite significant research on the topic, there is not a widely accepted theory of flow resistance for channels with large roughness, for example, boulder-mantled channels (Ferguson, 2007; Nitsche et al., 2012; Powell, 2014; Schneider et al., 2015; Shobe et al., 2021).

Many theoretical treatments of flow resistance in relatively shallow, rough channels attribute the increased flow resistance to form drag on large roughness elements (Nitsche et al., 2012; Shobe et al., 2021), which results from the need for water to flow around roughness elements. Features such as boulders, step and pool morphology, and large woody debris are often cited as potential sources of form drag (Powell, 2014). Even the relatively simple case of flow around isolated immobile boulders on a planar bed produces complicated, heterogeneous, and

© 2022 The Authors.

This is an open access article under the terms of the [Creative Commons Attribution-NonCommercial License](https://creativecommons.org/licenses/by-nc/4.0/), which permits use, distribution and reproduction in any medium, provided the original work is properly cited and is not used for commercial purposes.

unsteady flow fields (Papanicolaou & Tsakiris, 2017). To account for this properly in this study, a flow resistance model is developed using a double-average approach specifically designed to deal with spatial variability (Nikora et al., 2001). The resulting equations are averaged over the channel width and reach, allowing the flow to be treated as steady and uniform while still properly accounting for large boundary roughness.

The double-average approach has generally been applied at the local scale. It is used to compare theoretical expectations to experimental data that are spatially highly variable. Here local scale refers to a downstream-oriented vertical slice in a channel where flow variables are double-averaged over a volume that is small compared to the size of the channel. Double-averaging reveals consistent patterns in the flow that cannot be perceived in any one location, much like Reynolds (time) averaging reveals consistent patterns in turbulent flow despite short-term temporal variability due to turbulent fluctuations. Although the utility and importance of the double-average approach is clearly appreciated in the context of open channel flow (Brereton et al., 2021; Dey & Das, 2012; Kuwata & Kawaguchi, 2019; Nikora et al., 2001, 2007), it is the author's perspective that it is underutilized in the context of channel-scale variables. Here the channel scale refers to double-averaged variables which have been further averaged across the channel width and depth. This limits the ability to connect advances in open channel flow theory made through the double-average approach to field observations of natural rivers, which generally consist of measurements of channel-scale variables.

Here a connection is made between double-averaged local variables such as flow velocity and porosity, and channel-scale variables including hydraulic geometry (width, mean depth, mean flow velocity, flow resistance, and discharge) that are generally observable in the field. Using a shear partitioning approach guided by insight from the double-average approach, a semiempirical model for channel-scale flow resistance in a particular class of rough channels is derived. The channels in question are those where the dominant source of drag is form drag on large roughness elements. The model is then tested against a large data set of flow resistance in rough channels, and some of the critical variables are estimated.

2. Material and Methods

To test the theory developed below, a data set of paired measurements of mean flow velocity, surface flow width, mean flow depth, D_{84} (bed grain size), and channel slope is compiled from the literature. The relative flow depth ranges from $0.15 \leq H/D_{84} \leq 100$ and the grain size ranges from $0.02 \text{ m} \leq D_{84} \leq 1.5 \text{ m}$. The data set is composed of data from Williams and Rosgen (1989), Lepp et al. (1993), King (2004), and the data compilation of Rickenmann and Recking (2011). For channels with very large boundary roughness, the definition and measurement of flow depth becomes more challenging (Rickenmann & Recking, 2011). Here, this is accounted for by using only sites with direct velocity measurements, calculating the flow depth using $H = Q/UW$ and excluding the few data for $H/D_{84} < 0.2$. The data set and further details on how it was compiled have been made available in a data repository (Deal, 2021).

A smaller data set derived from Bathurst (1985) was constructed by taking the total cross-sectional area (A_T in Bathurst (1985)), flow cross-sectional area (A in Bathurst (1985)), relative roughness (A_w/A_T in Bathurst (1985)), and relative submergence (d/D_{84} in Bathurst (1985)) all from table 2 in Bathurst (1985). The mean flow depth was calculated as $H = A_c/W$ and the total cross-sectional area, A_T , was calculated by taking the cross-sectional area of the channel plus the upstream-facing area of the boulders. The channel boundary was defined by drawing straight lines between low points in the flow. The frontal area normalized by the flow cross-sectional area is compared to the relative flow depth.

3. Double-Averaged Navier-Stokes Approach and Definition of Channel-Scale Parameters

The double-averaged Navier-Stokes momentum equation (averaged in time and space) was first developed for atmospheric boundary layer flows (Raupach & Shaw, 1982; Wilson & Shaw, 1977) and has since been adapted to open channel flow (Giménez-Curto & Lera, 1996; Nikora et al., 2001, 2007, 2013; Whitaker, 1986). Double-averaging is an approach that lends itself to rough boundaries where the flow may vary significantly from one channel cross-section to another due to large roughness elements perturbing the flow. Importantly, for open channel flow, it has been demonstrated that double-averaged flow over rough boundaries resembles Reynolds-averaged

flow over smoother boundaries (Brereton et al., 2021; Dey & Das, 2012; Nikora et al., 2001, 2004; Sarkar & Dey, 2010).

In the double-averaged Navier-Stokes (DANS) momentum equation, a temporal and spatial decomposition is assumed for the flow velocity vector, $\mathbf{v} = \langle \bar{\mathbf{v}} \rangle + \tilde{\mathbf{v}} + \mathbf{v}'$. Here \mathbf{v} is the instantaneous velocity vector at a point and time (x, y, z, t) , the first right hand side term is the spatially and temporally (double) averaged velocity, where the overbar denotes an ensemble/time average, and the brackets denote a spatial average. The second and third terms are the temporal fluctuations due to turbulence, \mathbf{v}' , and spatial fluctuations over the averaging volume, $\tilde{\mathbf{v}}$, where by definition $\langle \tilde{\mathbf{v}} \rangle = \bar{\mathbf{v}}' = 0$. Spatial averaging occurs over the volume $V_o = Ldydz$ centered at x, y, z . Generally averaging is conceptualized as being taken over planes parallel to the boundary of the flow (Nikora et al., 2001, 2007). However, here curved channel profiles are considered and instead spatial averages are made over bars of downstream length L where $L \gg dy > dz$. The downstream length-scale is long enough that the statistics of boundary roughness converge, that is, much longer than the length-scale associated with boundary roughness. Further, the lateral length-scale is large enough to average over secondary circulation.

The DANS momentum equation of an incompressible Newtonian fluid for gravity-driven, steady, and uniform high Reynolds number flow in the x -direction down a reach-averaged slope of $S = \tan \theta \approx \cos \theta$ is as follows: (Giménez-Curto & Lera, 1996; Nikora et al., 2001, 2007)

$$\phi \rho g S = \frac{\partial}{\partial y} \left(\rho \phi \langle \overline{u'v'} \rangle + \rho \phi \langle \tilde{u}\tilde{v} \rangle \right) + \frac{\partial}{\partial z} \left(\rho \phi \langle \overline{u'w'} \rangle + \rho \phi \langle \tilde{u}\tilde{w} \rangle \right) + \nabla \cdot (\mu \nabla \phi \langle \bar{u} \rangle) + \phi \left(\langle \bar{f}_p \rangle + \langle \bar{f}_v \rangle \right), \quad (1)$$

where θ is the angle in the x - z plane between vertical and a vector normal to the boundary, ρ is the density of water, g is acceleration due to gravity, and μ is the viscosity of water. The porosity of the channel is represented by ϕ . Depending on the fraction of the averaging volume occupied by fluid versus rock, porosity takes on a value between 0 (100% rock-occupied) and 1 (100% fluid-occupied). It is an important parameter but at this point effectively unconstrained in natural channels. The variables x and $u(x, y, z)$ are the downstream flow direction and velocity, y and $v(x, y, z)$ are the cross-stream direction and velocity, and z and $w(x, y, z)$ are the vertical direction and velocity. The terms $\langle \overline{u'v'} \rangle$ and $\langle \overline{u'w'} \rangle$ are the Reynolds stresses due to turbulent fluctuations and the terms $\langle \tilde{u}\tilde{v} \rangle$ and $\langle \tilde{u}\tilde{w} \rangle$ are the dispersive stresses due to spatial variations in velocity.

The terms $\langle \bar{f}_p \rangle$ and $\langle \bar{f}_v \rangle$ are pseudo body forces per unit fluid volume (Brereton et al., 2021; Nikora et al., 2019). The form drag force,

$$\langle \bar{f}_p \rangle = -\frac{1}{V_f} \oint_s \bar{p} \hat{\mathbf{x}} \cdot \hat{\mathbf{n}} ds, \quad (2)$$

is the integral of time averaged pressure, \bar{p} , on all streamwise normal faces of the channel boundary (the surface s) per unit fluid volume, where $\hat{\mathbf{x}}$ is the unit vector in the x direction and $\hat{\mathbf{n}}$ is the unit vector normal to s . The term $\langle \bar{f}_v \rangle$ is the viscous drag force on the channel boundary per unit fluid volume:

$$\langle \bar{f}_v \rangle = \frac{1}{V_f} \oint_s \mu \nabla \bar{u} \cdot \hat{\mathbf{n}} ds. \quad (3)$$

The total drag force per unit volume is $\phi \langle \bar{f}_d \rangle = \phi \left(\langle \bar{f}_p \rangle + \langle \bar{f}_v \rangle \right)$.

Integrating over the flow depth from the deepest fluid-occupied point in the x - z plane z_b to the water surface z_s and dropping viscous terms yields a standard depth-integrated momentum balance for high Reynolds number, open channel flow (Chauvet et al., 2014; Knight, 1996; Morvan et al., 2008; Xu et al., 2020). In addition, here all variables are double-averaged:

$$\int_{z_b}^{z_k} \phi \langle \bar{f}_d \rangle dz = \rho g S h - \frac{\partial}{\partial y} \int_{z_b}^{z_s} \left(\rho \phi \langle \overline{u'v'} \rangle + \rho \phi \langle \tilde{u}\tilde{v} \rangle \right) dz \quad (4)$$

where z_k is the elevation of the top of the roughness layer, and the underbar represents a depth-averaged variable. The boundary stress, accounting for a laterally sloping channel boundary, is defined as the force dissipated on the boundary, which happens in the roughness layer

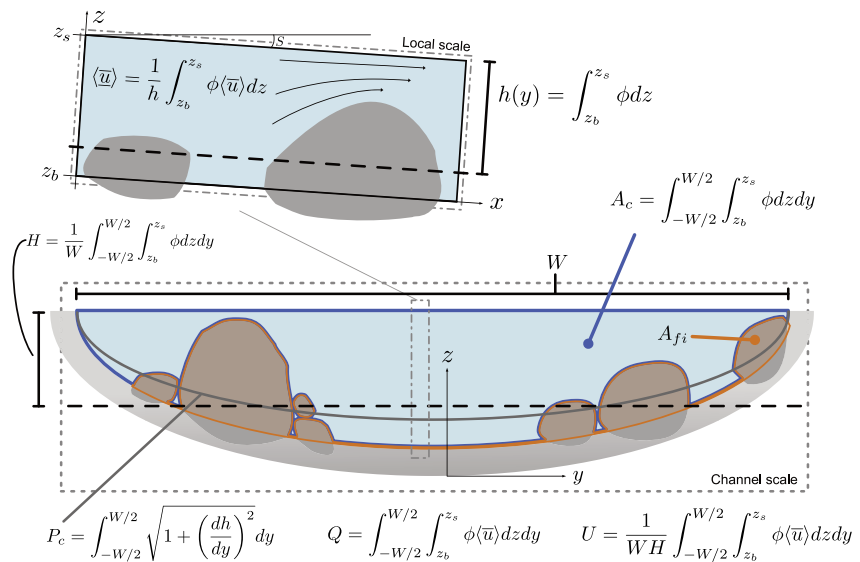


Figure 1. Schematic of rough channel showing both the local scale and channel scale. Local flow depth, h , and depth-averaged flow velocity, $\langle \bar{u} \rangle$ are defined as well as channel-scale width, W ; mean flow depth, H ; cross-sectional area, A_c ; channel perimeter, P_c ; water flux, Q ; mean flow velocity, U ; and upstream-facing area of i th roughness element, A_{fi} . The thick dashed black line represents the channel-averaged depth (shown in both panels) and the solid gray boundary labelled P_c represents the clear-water-equivalent depth along which the boundary perimeter length is measured (shown only in the lower panel).

$$\langle \bar{\tau}_o \rangle = \cos \varphi \int_{z_b}^{z_k} \phi \langle \bar{f}_d \rangle dz, \quad (5)$$

where φ is the angle in the x - y plane between vertical and a vector normal to the boundary. In this formulation, the shear stress is assumed to be distributed over the entire boundary, not accounting for porosity at the boundary. However, the boundary stress could equally be defined as $\langle \bar{\tau}_o \rangle = (\cos \varphi / \phi) \int_{z_b}^{z_k} \phi \langle \bar{f}_d \rangle dz$, which is the boundary stress focused onto just the fraction of the boundary occupied by fluid.

The boundary itself can be challenging to define for very rough channels (Smart et al., 2002). Here the double-averaged boundary is defined by the clear-water-equivalent flow depth for each slice in the x - z plane (Kuwata & Kawaguchi, 2019), where the clear-water-equivalent flow depth is the depth of the flow assuming no roughness, shown as a gray solid line labelled P_c in Figure 1. This is the integral of the porosity over the flow depth

$$h(y) = h_l + \underline{\phi} k = \int_{z_b}^{z_s} \phi dz \quad (6)$$

where $k = z_k - z_b$ is the thickness of the roughness layer, $\underline{\phi} = (1/k) \int_{z_b}^{z_k} \phi dz$ is the depth-averaged porosity over the roughness layer, and $h_l = z_s - z_k$ is the remaining flow depth above the roughness layer.

By integrating Equation 4 across the channel width, the boundary stress averaged along the double-averaged channel boundary, τ_o , is shown to be

$$\tau_o = \rho g S R. \quad (7)$$

Where a symmetrical channel (in a double-averaged sense) is assumed, the integral of the lateral stress sums to zero, and $R = A_c / P_c$ is the hydraulic radius. The same approach can be used to calculate several other important channel-scale variables, such as the mean flow depth for the channel, given in Figure 1 and Appendix A.

This definition of the average boundary stress and the boundary itself contrasts with that of Smart et al. (2002), for example, who use the volumetric hydraulic radius, which is equal to the average flow depth $R_v = H = A_c / W$. The stress defined using the flow width is a maximum bound on the double-averaged stress dissipated on the actual channel boundary because any curved channel perimeter will be larger than the channel width. Although

the volumetric hydraulic radius, R_v , is useful for being simple to measure, the hydraulic radius in Equation 7 is preferred here because it is consistent across channels of small and large roughness. In practice, it is likely that the two measures are nearly interchangeable.

4. Flow Resistance

The flow resistance derives from the ratio of the shear stress to the dynamic pressure, $\frac{1}{2}\rho\langle\bar{u}\rangle^2$,

$$\frac{\langle\bar{\tau}_o\rangle/\cos\varphi}{\rho\langle\bar{u}\rangle^2} = \frac{\langle\bar{C}_f\rangle}{2} = \left(\frac{\langle\bar{u}\rangle}{\langle\bar{u}_*\rangle}\right)^{-2} \quad (8)$$

where $\langle\bar{u}\rangle(y) = (1/h)\int_{z_b}^{z_s}\phi\langle\bar{u}\rangle dz$ is the local depth-averaged velocity, $\langle\bar{u}_*\rangle = \sqrt{\langle\bar{\tau}_o\rangle/\rho\cos\varphi}$ is the local shear or friction velocity, and $\langle\bar{C}_f\rangle$ is the local coefficient of drag.

Using the same DANS momentum equation (Equation 1), the boundary stress has been shown to be equal to the sum of different sources of friction (Kuwata & Kawaguchi, 2019; Nikora et al., 2019) based on a successful approach for Reynolds averaged flows (Fukagata et al., 2002). Here, the formulation from Nikora et al. (2019) is given but both formulations are similar

$$\frac{\langle\bar{\tau}_o\rangle}{\cos\varphi} = \frac{3}{N_o h} \left[\mu\phi\langle\bar{u}\rangle - \frac{1}{h} \int_{z_b}^{z_s} (z_s - z) \rho\phi\langle\bar{u}'w'\rangle dz - \frac{1}{h} \int_{z_b}^{z_s} (z_s - z) \rho\phi\langle\bar{u}\bar{v}\bar{v}\rangle dz + \frac{F_{3D}}{2h} \right] \quad (9)$$

where the first term represents the viscous drag and the second term the turbulent stress. The third term accounts for dispersive stresses, including both spatial variations in flow velocity due to spatially varying bed geometry and spatial variations due to secondary circulation. The final term collects other 3D flow terms such as spatial deviations in inertial and pressure forces due to local temporal and spatial accelerations in fluid velocity. These terms and the normalizing factor, N_o , are given in Appendix B.

Equation 9 and the DANS framework in general are important for several reasons. First, a single framework can describe drag in simple 2D flows as well as drag due to spatial pressure fluctuations and spatial and temporal fluid accelerations that may be important in very rough, 3D flows (Kuwata & Kawaguchi, 2019; Nikora et al., 2019). Second, it shows that even with a careful accounting of the flow, the drag can be considered a linear sum of different components, each attributable to a different phenomenon:

$$\langle\bar{C}_f\rangle = \sum_i \langle\bar{C}_{f_i}\rangle \quad (10)$$

where i sums over the different terms contributing to flow resistance.

The channel-scale flow resistance is the average of the local flow resistance:

$$C_f = 2\left(\frac{U}{u_*}\right)^{-2} = \left(\frac{1}{W} \int_{-W/2}^{W/2} \left(\sum_i \langle\bar{C}_{f_i}\rangle\right)^{-\frac{1}{2}} dy\right)^{-2} \quad (11)$$

where $u_* = \sqrt{\tau_o/\rho} = \sqrt{gRS} \approx \sqrt{gHS}$. Under the assumptions that the boundary stress is, in a double-averaged sense, approximately constant across the channel width ($\nabla\langle\bar{\tau}_o\rangle \approx 0$ and $u_* \approx \langle\bar{u}_*\rangle$) and that the majority of the resistance comes from the bottom roughness and not channel walls, this can be simplified to $C_f \approx \sum_i \langle\bar{C}_{f_i}\rangle$ and the channel-scale flow resistance can be cast as follows:

$$\frac{U}{u_*} = \frac{1}{\sqrt{\frac{1}{2} \sum_i \langle\bar{C}_{f_i}\rangle}} \quad (12)$$

This is strongly reminiscent of the empirical variable power equation (VPE) (Ferguson, 2007):

$$\frac{U}{u_*} = \frac{1}{\sqrt{\frac{1}{2}C_{f_{smooth}} + \frac{1}{2}C_{f_{rough}}}}; \quad C_{f_{smooth}} = \frac{2}{a_1^2} \left(\frac{H}{k}\right)^{-1/3}; \quad C_{f_{rough}} = \frac{2}{a_2^2} \left(\frac{H}{k}\right)^{-2} \quad (13)$$

as well as several other recent formulations for flow resistance across smooth and rough channels (Cheng, 2017; Rickenmann & Recking, 2011). Here $C_{f,smooth}$ and $C_{f,rough}$ are the channel drag coefficients for smooth and rough boundaries, respectively (Ferguson, 2007). These equations capture the increase in flow resistance for channels with rough boundaries, effectively increasing the exponent in the relationship $U/u_* \propto (H/D_{84})^r$ as roughness increases. Here it is pointed out that this form probably arises more or less inevitably due to the additive nature of the coefficients of various sources of drag and the inverse-square relationship between flow velocity and the total drag coefficient.

4.1. Flow Resistance in Open Channel Flow

If the profile of average flow velocity as a function of depth $\langle \bar{u} \rangle(y, z)$ is known, the local drag coefficient can be derived by integrating $\langle \bar{u} \rangle(y, z)$ with depth (Smart et al., 2002). To find $\langle \bar{u} \rangle(y, z)$, the flow can be divided into four layers (Nikora et al., 2001): From the water surface down there is an outer layer, a logarithmic layer, a roughness layer, and a subsurface layer. However, for open channel flow in natural rivers, the outer layer is often ignored and the logarithmic layer is generally considered to extend all the way to the surface (Schlichting & Gersten, 2015). The flow velocity in the logarithmic layer is well captured by the classic log law of the wall (Chung et al., 2021), which can be derived using the Boussinesq hypothesis and assuming a turbulent mixing length-scale that is proportional to the height above the bed (Keulegan, 1938). This is well known but the details and standards have continued to evolve, as nicely described in several recent reviews (Brereton et al., 2021; Chung et al., 2021), so a short summary is given below.

The presence of a roughness layer does not appear to modify the flow in the logarithmic layer substantially but simply sets the boundary condition for the logarithmic profile (Chung et al., 2021; Flack & Schultz, 2014; Lamb et al., 2017b). It has been well established that for rough boundaries where there is sufficiently deep flow above the highest portions of the roughness layer, a logarithmic layer still develops that is well described by (Brereton et al., 2021; Chung et al., 2021; Dey & Das, 2012; Flack & Schultz, 2014; Lamb et al., 2017b; Nikora et al., 2001, 2004, 2007 and Sarkar & Dey, 2010):

$$\frac{\langle \bar{u} \rangle}{\langle \bar{u}_s \rangle} = \frac{1}{\kappa} \ln \left(\frac{z-d}{k_s} \right) + B_s = \frac{1}{\kappa} \ln \left(\frac{e^{\kappa B_s}}{k_s} (z-d) \right) \quad (14)$$

where k_s is the effective sand grain roughness and B_s is a function of $\rho k_s \langle \bar{u}_s \rangle / \mu$ that assumes a constant value of ~ 8.5 for hydraulically rough flows ($\rho k_s \langle \bar{u}_s \rangle / \mu > 100$), a criterion expected to be met in effectively all natural channels. Integrating $B_s = 8.5$ into the natural log leads to a factor of 30 ($e^{\kappa B_s} \approx 30$), where it is assumed that $\kappa = 0.41$.

The variable d is a zero-plane displacement that accounts for modifications in the flow close to the top of the roughness layer due to flow in the roughness layer (Chung et al., 2021; Lamb et al., 2017b). It is generally a small correction that can be ignored if the flow of interest is far from the roughness layer. Using a modified mixing-length model Lamb et al. (2017b) show that $d = -k_s e^{\kappa (\langle \bar{u}_0 \rangle / \langle \bar{u}_s \rangle - B_s)}$, where $\langle \bar{u}_0 \rangle$ is the flow velocity at the top of the roughness layer. This flow velocity becomes relevant when there is significant flow through the roughness and subsurface layers.

In Equation 14, the roughness is represented with the effective sand grain roughness length-scale k_s . If the roughness is instead described with a measure of the actual boundary roughness such as the standard deviation of bed elevation or characteristic grain size (e.g., D_{50} or D_{84}), the flow velocity can be written instead in terms of k' and B_k , where k' is the measure of bed roughness used. This is less useful because, in general, B_k is not known for an arbitrary surface, even for hydraulically rough flows (Brereton et al., 2021), and there is not a unique relationship between k' and k_s (Kuwata & Kawaguchi, 2019).

The mean velocity over the logarithmic layer is as follows (Keulegan, 1938; Smart et al., 2002):

$$\frac{\langle \bar{u} \rangle}{\langle \bar{u}_s \rangle} = \frac{1}{h_l} \int_{k_s+d}^{k_s+h_l} \frac{1}{\kappa} \ln \left(\frac{e^{\kappa B_s}}{k_s} (z-d) \right) dz = \frac{1}{\kappa} \ln \left(\frac{e^{\kappa B_s-1} h_l}{k_s} \right) + \mathcal{O} \left(\frac{k_s}{h_l} \right) \quad (15)$$

where h_l is the thickness of the logarithmic layer, $e^{\kappa B_s-1} \approx 12$ and integration is from just below the effective sand roughness height $\left(z = k_s + d = k_s \left(1 - e^{\kappa (\langle \bar{u}_0 \rangle / \langle \bar{u}_s \rangle - B_s)} \right) \right)$. If the thickness of the logarithmic layer is much larger than the effective sand roughness layer ($h_l \gg k_s$), then the thickness and average flow velocity of the logarithmic layer become good approximations of the entire flow depth.

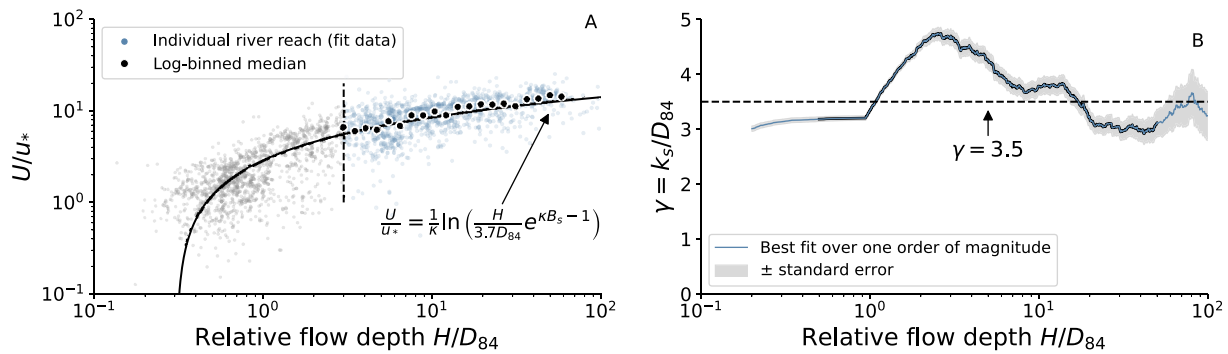


Figure 2. Comparing log law of the wall depth velocity model to flow resistance data. Panel A shows a best fit of Equation 15 to the data set described in Section 2 for relative flow depths of $H/D_{84} \geq 3$. The only fit parameter is $\gamma = 3.7 \pm 0.14$, where the uncertainty represents one standard error of the best fit. Panel B shows the best fit γ value over a moving window of one order of magnitude ($\pm 1/2$ order of magnitude centered on each H/D_{84} value). The blue line shows the best fit value, the gray region shows the bounds of \pm one standard error, and the black line shows the range of data for which there were data over the entire one order of magnitude window.

Figure 2 shows Equation 15 fit to the flow resistance data set described in Section 2 for relative flow depths greater than $H/D_{84} \geq 3$ using a nonlinear least squares method. The flow resistance model fits the data well, as expected, and the best fit value for $\gamma = k_s/D_{84}$ is $\gamma = 3.7 \pm 0.14$. Figure 2b shows the best fit value of γ when the data are fit over a moving window of just one order of magnitude, demonstrating that it is approximately in the range $3 \leq \gamma \leq 4.5$ and does not depend strongly on the bounds of the fit data.

4.2. Flow Resistance for Rough Boundaries

At some point, as the roughness layer occupies a larger and larger fraction of the flow depth, the logarithmic layer will disappear and the bulk flow velocity is determined by flow in the roughness and subsurface layers. The logarithmic layer is expected to persist until $h_1/k \approx 15$ (Flack & Schultz, 2014); however, experiments have shown that it can be observed for relative flow depths as small as $h_1/k \approx 1$ (Lamb et al., 2017b). Regardless of whether the logarithmic layer persists or not, when the roughness layer thickness is a large fraction of the overall flow depth, equating the logarithmic layer with the entire flow depth will become a poor approximation and a transition to roughness and subsurface layer dominated flow resistance will begin.

Flow in the roughness layer and subsurface layer is not as well understood as in the logarithmic layer, though under certain conditions particular depth-velocity profiles are predicted and observed, such as linear or exponential profiles (Nikora et al., 2004). Similarly, there are some predictions of flow through the subsurface layer, principally depending on non-Darcy (i.e., turbulent) flow through porous media, modeled by the Darcy-Forchheimer equation (Lamb et al., 2017b; Luo et al., 2022). Despite these promising results, research has not consolidated enough for a simple, useable, and well-tested model of mean flow velocity in the roughness and subsurface layers to emerge.

In the absence of a useable theory, empirical power-law models are used to capture the flow resistance in channels with rough boundaries (Ferguson, 2007; Rickenmann & Recking, 2011). These models generally take the form

$$C_f = k_f \left(\frac{H}{k_s} \right)^{-2r} \quad (16)$$

where r is observed to be approximately 1 in compilations of natural channels with rough boundaries (Ferguson, 2007; Rickenmann & Recking, 2011; Smart et al., 2002).

Using a shear partitioning approach guided by insight from the DA approach, a semiempirical prediction for the value of the exponent r is laid out below. The prediction should be valid in channels where the majority of the drag comes from pressure drag on large roughness elements, referred to as boulders. To do this, the dissipation of momentum on the boundary can be divided into the momentum dissipated throughout the flow on boulders, if any exist, denoted by τ_r , plus the momentum dissipated close to the boundary of the channel, denoted by τ_b .

Note that in both regions, momentum is dissipated through a combination of form and skin drag. However, in this way, the detailed approaches (Kuwata & Kawaguchi, 2019; Nikora et al., 2019) can be reconciled with intuitive approaches that partition drag. In this perspective the average boundary stress is

$$\tau_o = \frac{1}{P_c} \int_{-\frac{W}{2}}^{\frac{W}{2}} \left[\int_{z_b}^{z_c} \phi \langle \overline{f_d} \rangle dz + \int_{z_c}^{z_s} \phi \langle \overline{f_d} \rangle dz \right] dy = \tau_b + \tau_r \quad (17)$$

where z_c is a depth close to the boundary that distinguishes between boundary drag and drag on boulders.

If there are boulders or other large roughness elements protruding into the flow, the physical mechanisms responsible for the spatial distribution of flow velocities are captured by Equation 9. However, the dissipation of momentum on the large roughness elements can be roughly estimated using the average pressure force on upstream-facing roughness elements per unit volume, F_p

$$\tau_r = \frac{1}{P_c} \int_{-\frac{W}{2}}^{\frac{W}{2}} \int_{z_c}^{z_s} \oint_s \frac{-\overline{p}\mathbf{x} \cdot \hat{\mathbf{n}}}{V_o} ds dz dy = \frac{1}{P_c} \int_{-\frac{W}{2}}^{\frac{W}{2}} \left(h\phi \langle \overline{f_p} \rangle + \epsilon_o \right) dy = \frac{c_o}{P_c} \left(WHF_p + W\epsilon_o \right) \quad (18)$$

This assumes that the drag force results predominantly from form drag, $\langle \overline{f_p} \rangle$, which may not be completely valid, even in very rough channels (Nikora et al., 2019). Two further approximations are made here. The first approximation is that the depth-integrated pressure force per unit fluid volume, $h\phi \langle \overline{f_p} \rangle$, can be substituted for the pressure force per unit fluid volume integrated from z_c to z_s . This approximation becomes reasonable if the boundary elevation z_c is close to the bed elevation z_b . This leads to the term ϵ_o , which is assumed to be small.

The second approximation is that $H F_p \approx \int_{-W/2}^{W/2} h\phi \langle \overline{f_p} \rangle dy$, which is only strictly true if $\phi \langle \overline{f_p} \rangle$ does not depend on depth. This is dealt with by adding an unknown coefficient that compensates for how $\phi \langle \overline{f_p} \rangle$ varies with distance from the bed. This added coefficient will depend strongly on the geometry of the boundary and the flow.

The average pressure force on upstream-facing area of boulders per unit volume can be written as follows:

$$F_p = \frac{C_D \frac{\rho}{2} U_p^2 A_f}{H A_o} \quad (19)$$

where A_f is the upstream-facing area in an average cross-section of downstream extent k_s , $A_o = Wk_s$ is the channel bed area associated with an average channel cross-section, C_D is the average drag coefficient on a boulder, and

$$U_p^2 = \frac{1}{W} \int_{-W/2}^{W/2} \frac{1}{h} \int_{z_c}^{z_s} \frac{1}{V_o} \oint_s \overline{u}^2 ds dz dy \quad (20)$$

is the effective velocity that should give the correct drag when multiplied by the upstream-facing area in a channel reach. Here it is assumed that this velocity scales with the mean channel-scale velocity, $U_p = \sqrt{c_1} U$, though the coefficient will necessarily depend on the distribution of velocity and roughness element surface area with depth; therefore c_1 should be highly sensitive to the channel geometry.

With these approximations, and using the relationships $\tau_o = \rho u_*^2$ and $C_f = 2(u_*/U)^2$:

$$\tau_r \approx c_o H F_p = C_D \frac{A_f}{A_o} \frac{c_o c_1 \rho}{2} U^2 = \tau_o \frac{c_o c_1 c_d}{C_f} \frac{A_f}{A_o} \left(\frac{H}{D_{84}} \right)^{\frac{3}{2}} \quad (21)$$

where the drag coefficient on a single boulder is approximated as $C_D = c_d (H/D_{84})^{-3/2}$ (Lamb et al., 2017a). This is an empirical model for the drag coefficient based on observations of a single roughness element protruding from the bed. The experiments of Lamb et al. (2017a) use only single grain size, D , which is not strictly comparable to D_{84} used here. Therefore the coefficients and range of applicability will be different than in Lamb et al. (2017a). The range of relative flow depths (H/D_{84}) where this model is applicable is likely to be larger, as D_{84} does not represent the largest grain size, so $D_{84} < D$.

Using geometrical arguments (Appendix C), the upstream-facing boulder area per unit planform channel area, also known as the frontal solidity, λ_f (Chung et al., 2021), is

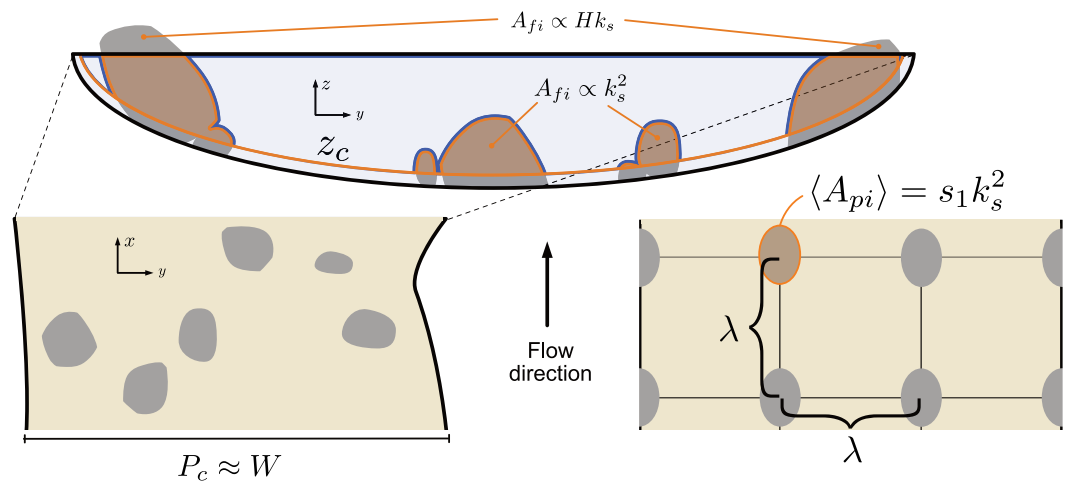


Figure 3. Schematic of river channel with large roughness elements, for example, boulders looking downstream (top) and from above (bottom). Shown is the elevation z_c around which the shear partitioning is based, the difference between boulders whose upstream-facing area should scale with Hk_s and those who should scale with k_s^2 , and the definition of the boulder planform density based on an average spacing of λ (see Appendix C).

$$\lambda_f = \frac{A_f}{A_o} = s\lambda_p \left(\frac{H}{\gamma D_{84}} \right)^{1-a} \quad (22)$$

where λ_p is the planform boulder area per unit planform channel area, also known as planform solidity (Chung et al., 2021), s is a factor that depends on the average boulder shape, and a controls how the upstream-facing boulder area increases when the channel becomes rougher. As illustrated in Figure 3, if the flow resistance depends on a few boulders significantly larger than the flow depth, the expectation is that the upstream-facing area scales with $k_s H$ and $a = 0$. If instead the area lost by large boulders protruding more and more from progressively shallower flows is compensated by smaller roughness elements, the expectation is that $A_f \sim k_s^2$ and $a = 1$.

If the drag predominantly comes from drag on roughness elements throughout the depth of the flow (e.g., $\tau_o \approx \tau_r$), then Equation 21 can be combined with Equation 22 to yield

$$C_f = c_o c_1 c_d s \lambda_p \gamma^{a-1} \left(\frac{H}{D_{84}} \right)^{-(a+\frac{1}{2})} \quad (23)$$

and consequently

$$\frac{U}{u_*} \approx \frac{1}{\sqrt{\frac{1}{2} c_o c_1 c_d s \lambda_p \gamma^{a-1}}} \left(\frac{H}{D_{84}} \right)^{\frac{1+2a}{4}} \quad (24)$$

5. Results

To estimate the value of a in natural channels, it can also be shown that the average upstream-facing roughness area per unit channel cross-section area is (Appendix C):

$$\frac{A_f}{A_c} = s\lambda_p \left(\frac{H}{\gamma D_{84}} \right)^{-a} \quad (25)$$

Using a data set of A_f and A_c from Bathurst (1985), I find that there is a consistent power-law relationship between A_f/A_c and H/D_{84} and that $a = 1.10 \pm 0.03$ and $s\lambda_p \gamma^{1.1} = 0.63 \pm 0.01$, see Figure 4a.

Using the larger data set discussed in Section 2, a power-law is fit to the flow resistance observations with relative flow depths between $0.2 \leq H/D_{84} \leq 2$ using a nonlinear least squares method, for a best fit exponent of

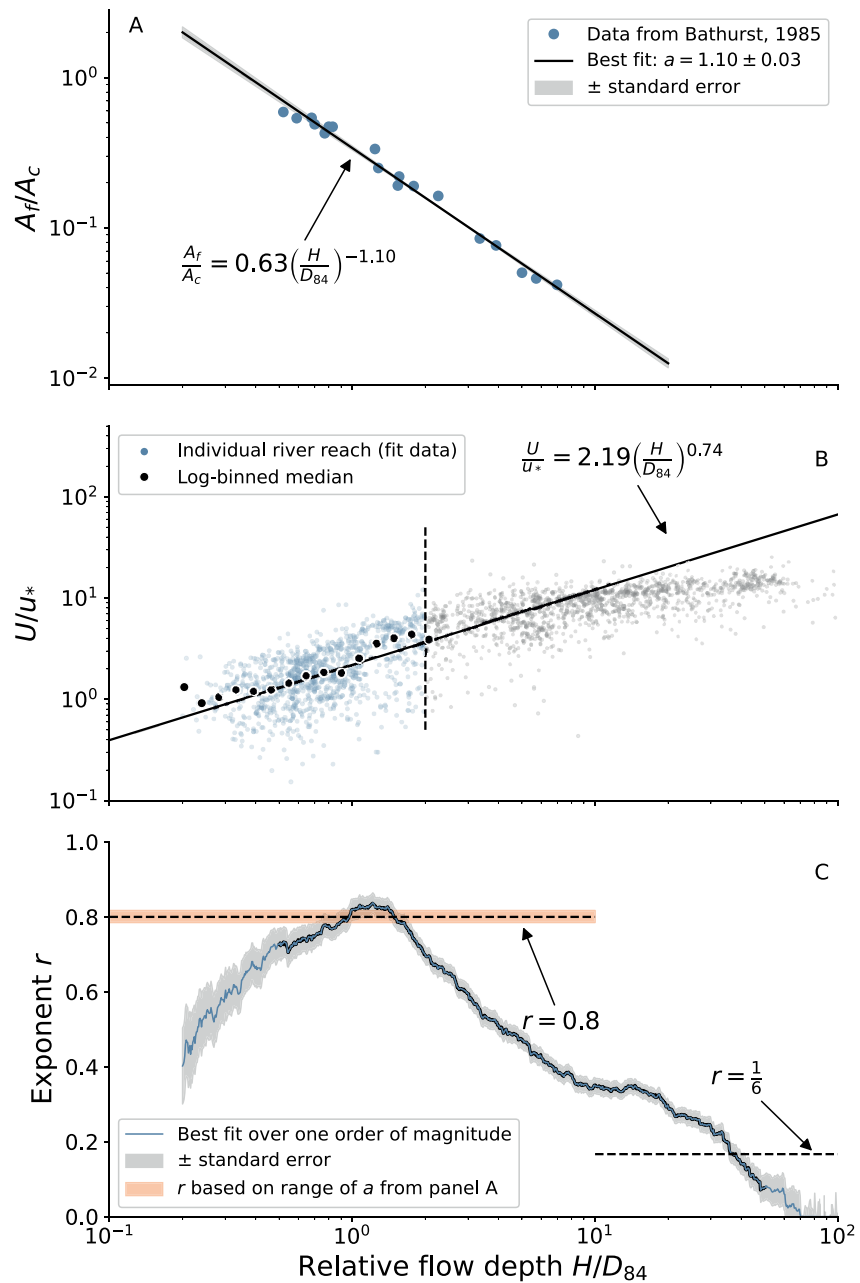


Figure 4. Panel A shows the best fit of the ratio of upstream-facing roughness element area in an average cross-section, A_r , to the flow area in an average cross-section, A_c , as a function of the relative flow depth using a nonlinear least squares method. Panel B shows a power-law best fit to the flow resistance observations from the larger data set discussed in Section 2 with relative flow depths smaller than $H/D_{84} \leq 2$ using a nonlinear least squares method. The best fit exponent is $r = 0.74 \pm 0.03$. In panel C, to test the effect of choosing an upper limit for the fit data, the data are fit in a moving window of one order of magnitude. The blue line shows the best fit value, the gray region shows the bounds of \pm one standard error, and the black line shows the range of data for which there were data over the entire one order of magnitude window.

$r = 0.74 \pm 0.03$, see Figure 4b. To test the effect of the chosen data limits on the value of the exponent, Figure 4c shows the best fit exponent when only data within a moving window of one order of magnitude are used. For relative flow depths from $1/2 \leq H/D_{84} \leq 2$, $r \geq 3/4$.

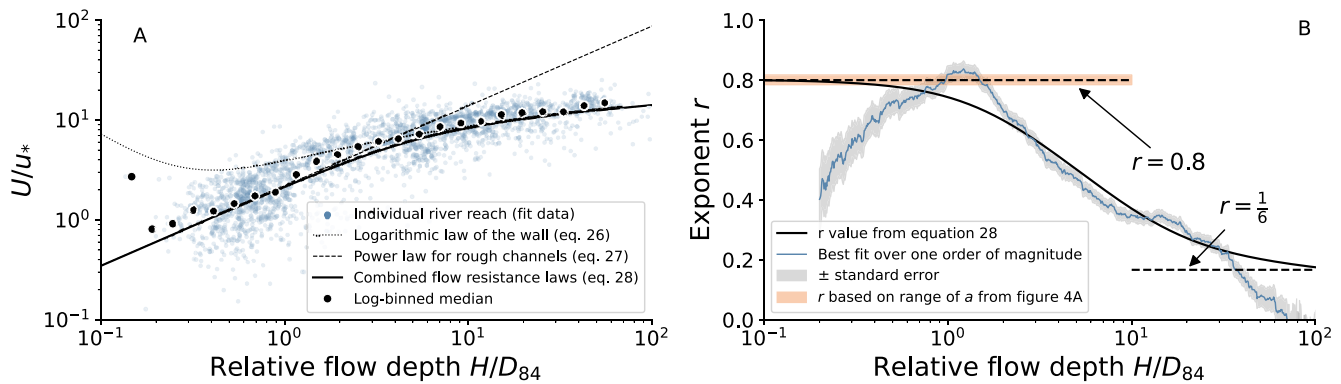


Figure 5. Panel A shows the fit of the flow resistance models for smooth channels (Equation 26), rough channels (Equation 27) and the proposed unified model (Equation 28) compared to the compiled dataset of flow resistance in natural rivers. Panel B shows the best fit value of the exponent r fit as in Figure 4c compared to the value of r predicted by Equation 28.

The value of r predicted from fitting a to the Bathurst (1985) data set is $r = 0.8 \pm 0.02$, which is approximately in line with the observed range of r for rough boundaries, as well as the value of r found by others (Ferguson, 1986; Rickenmann & Recking, 2011; Smart et al., 2002).

Using the above values, the flow resistance coefficients for smooth and rough channels can be defined as follows:

$$C_{f_{smooth}} = 2 \left(\frac{1}{\kappa} \ln \left(3.3 \frac{H}{D_{84}} \right) + \frac{D_{84}}{H} \right)^{-2} \quad (26)$$

where the $\mathcal{O}(D_{84}/H)$ term is taken to be simply D_{84}/H and

$$C_{f_{rough}} = c_o c_1 c_d s \lambda_p \gamma^{a-1} \left(\frac{H}{D_{84}} \right)^{-(a+\frac{1}{2})} = \frac{2}{2.19^2} \left(\frac{H}{D_{84}} \right)^{-1.6} \quad (27)$$

where $a = 1.1$. The above two models can be combined using Equation 12. Theoretically, the unified model should consist of the inverse of the square root of the sum of squared terms. However, using a higher power gives a model that transitions more rapidly from one end member model to the other, and fit the data better. In the interest of a more functional model, here the fourth power is used:

$$\frac{U}{u_*} = \frac{1}{\sqrt[4]{\left(\frac{1}{\kappa} \ln \left(3.3 \frac{H}{D_{84}} \right) + \frac{D_{84}}{H} \right)^{-4} + .043 \left(\frac{H}{D_{84}} \right)^{-3.2}}} \quad (28)$$

The comparison between this unified model and the data set is shown in Figure 5.

6. Discussion

Despite the caveat that the Bathurst (1985) data set is quite small, the fit values of $a = 1.10$ and $s \lambda_p \gamma^{1.1} = 0.63$ lead to some interesting interpretations. The observation that $a \approx 1$ implies that the upstream-facing roughness area of an average roughness element increases as $\sim k_s^2$. This means that as large boulders or other roughness elements protrude from the flow for progressively shallower flows, the lost area is supplemented by other sources. This also implies that the upstream-facing roughness area per unit channel width normalized by the roughness length-scale (i.e., per average cross-section) is a constant $\left(\frac{A_f}{k_s W} \approx 0.15 \right)$.

Similarly, when $a \approx 1$, the frontal and planform solidities are directly proportional to one another, and this relationship depends only on the details of boulder shape, rather than on any properties of the flow, such as relative flow depth. The frontal and planform solidity have been shown to be important in determining the drag properties

of a boundary (Chung et al., 2021), and it would be significant if their relationship to one another were both constrained and independent of details of the flow in natural channels.

In addition the value of frontal solidity can be inferred from the coefficient of the best fit in Figure 4a, which gives $\lambda_f \approx s\lambda_p \approx 0.63/\gamma \approx 0.15\text{--}0.2$. This assumes that the value of γ fit for relatively deep flows holds for relatively shallow flows as well. Interestingly, if this value is correct, it is in the range of values for frontal solidity that produce maximal flow resistance (Chan et al., 2015; MacDonald et al., 2018). Beds with either significantly higher or lower roughness element density exhibit lower flow resistance. If there is a mechanism whereby channels optimize for maximum flow resistance, one would expect $0.1 \leq \lambda_f \leq 0.3$.

Natural surfaces often have special properties such as being fractal or self-affine (Cox & Wang, 1993; Power & Tullis, 1991; Stewart et al., 2019). Also, natural channels are regularly modified by the flow, potentially driving them to exhibit similar properties across different rivers (Aberle & Nikora, 2006) by, for example, maximizing or minimizing certain properties. In addition to the interesting relationships between frontal and planform solidity and flow resistance, there are several other lines of evidence to support the viewpoint that natural channels converge on similar drag behavior. Such effects could potentially simplify the prediction of flow resistance in rough channels.

First, it has been established that a simple measure of bed morphology such as maximum or standard deviation of bed elevation cannot fully describe the bed roughness (Breerton et al., 2021; Chung et al., 2021; Kuwata & Kawaguchi, 2019). Based on this alone, it is unlikely that there is a unique relationship between characteristic grain size or the standard deviation of bed height and k_s for natural river channels. Yet, the fact that a relatively consistent, albeit noisy, relationship is frequently observed (the oft quoted $k_s \approx 3D_{84}$ (Hey, 1979; Lamb et al., 2017b; Figure 2) suggests some amount of convergence in the bed morphology of natural rivers (Aberle & Nikora, 2006; Stewart et al., 2019).

Also in support of these ideas is the fact that the model derived above, which has many approximations, seems to match well with observations. Several of the approximations made, such as relating the mean flow velocity, U , to the average flow velocity impinging on roughness elements, U_p , should be highly sensitive to bed geometry. The observation that the exponent a in the Bathurst (1985) data set and the exponent r in the larger data set of flow resistance match according to Equation 23 implies that the coefficients c_1 , c_d , s , and γ are not changing too strongly as channels become rougher. There is spread in flow resistance for any given channel at a given relative flow depth, so it may be that bed geometries are changing from channel to channel. However, this variability occurs around a well-behaved trend in the data, implying the existence of some consistent, approximate patterns.

The model of drag on isolated boulders from Lamb et al. (2017a) is critical for producing the observed match between the exponents a and r . This is a fully empirical model based on flume experiments with relatively simple geometry that has not been tested in natural channels. While this is an important caveat, other measures of drag on individual grains, although more indirect, have made qualitatively similar observations that the drag coefficient increases as the relative flow depth decreases (Carling et al., 2002; Lawrence, 2000). Still, changes in the model proposed by Lamb et al. (2017a) due to more data or more realistic conditions will result in direct changes to the model proposed in Equation 23.

It is important to note that the model proposed above should not describe all rough channel bed configurations. Flow resistance due to form drag on isolated large roughness elements such as boulders is just one of a variety of ways to produce flow resistance in rough channels (Powell, 2014). Lamb et al. (2017b), for example, describe a rough channel with no large roughness elements protruding into the flow and predict a model for flow resistance that also explains the observations in Figure 4b, but for different reasons.

The data set presented in Bathurst (1985) is particularly detailed in that it allows for the estimation of A_f . Though it is small, so the interesting and potentially significant implications of the results in Figure 4a could be taken more seriously if tested against a larger data set. This would be an ideal direction for future work.

Finally, the concept of steady and uniform in a double-average sense implicitly makes the assumption that even in very rough channels, the effect of the roughness on the flow, in terms of spatial pressure, velocity, and acceleration fluctuations, converges to an average over large enough downstream length-scales. Certain geometries, such as a consistent downstream increase or decrease in channel slope, cannot be meaningfully described as steady and uniform. Therefore, although the double-average approach allows for the concept of steady, uniform flow to be applied to a much wider range of natural channels, there are limitations to where it can simplify understanding of open channel flow.

7. Conclusions

Using a shear partitioning approach guided by insight from the double-average approach, a model is derived for channel-scale flow resistance for channels where the dominant source of drag is form drag on boulders. The model is then tested against a large data set of flow resistance in rough channels, and values for important exponents and coefficients are shown to be consistent with both observations as well as previous estimates.

Notably, several of the coefficients in the proposed model should depend on the channel geometry. Yet the observations imply that these coefficients do not vary strongly between different channels. This suggests that there may be characteristics of natural river channels with rough boundaries that are relatively uniform across different channels, leading to consistency in the behavior of flow resistance. This demonstrates that when averaged over the correct length-scale, the effects of significant spatial variability, even at scales as large as the channel width, can converge to a uniform and perhaps predictable effect.

Appendix A: Channel-Scale Variables

The average boundary stress, τ_o , is found by integrating the shear stress across the channel width

$$\tau_o = \frac{1}{P_c} \int_{-W/2}^{W/2} \frac{\langle \tau_o \rangle}{\cos \phi} dy \quad (\text{A1})$$

where the perimeter is defined as (and noting that $1/\cos \phi = \sqrt{1 + (dh/dy)^2}$)

$$P_c = \int_{-W/2}^{W/2} \sqrt{1 + \left(\frac{dh}{dy}\right)^2} dy \quad (\text{A2})$$

The hydraulic radius is defined as the ratio of the channel cross-sectional area to channel perimeter $R = A_c/P_c$ where cross-sectional area is

$$A_c = \int_{-W/2}^{W/2} h dy, \quad (\text{A3})$$

The lateral stress is defined as the sum of the lateral turbulent and dispersive stresses

$$\langle \tau_{xy} \rangle = -\rho \left(\langle u'v' \rangle + \langle \tilde{u}\tilde{v} \rangle \right) \quad (\text{A4})$$

Further $\langle \tau_{xy} \rangle = (1/h) \int_{z_b}^{z_s} \phi \langle \tau_{xy} \rangle dz$ is the depth-averaged lateral shear stress, where the depth-averaging is denoted with an underbar.

Using the above definitions and integrating the momentum balance across the channel width, W , yields a standard expression for open channel flow

$$\tau_o = \frac{1}{P_c} \int_{-W/2}^{W/2} \left(\rho g S h + \langle \tau_{xy} \rangle \right) dy = \rho g S \frac{A_c}{P_c} = \rho g S R \quad (\text{A5})$$

where a symmetrical channel (in a double-averaged sense) is assumed and the integral of the lateral stress sums to zero.

The same approach can be used to calculate several other important channel-scale variables, such as the mean flow depth for the channel, (all given in Figure 1)

$$H = \frac{1}{W} \int_{-W/2}^{W/2} \int_{z_b}^{z_s} \phi dz dy = \frac{A_c}{W} \quad (\text{A6})$$

the average water flux,

$$Q = \int_{-W/2}^{W/2} \int_{z_b}^{z_s} \phi \langle \bar{u} \rangle dz dy \quad (\text{A7})$$

and the average flow velocity,

$$U = \frac{1}{WH} \int_{-W/2}^{W/2} \int_{z_b}^{z_s} \phi \langle \bar{u} \rangle dz dy = \frac{Q}{A_c} \quad (\text{A8})$$

Appendix B: Drag Terms

The additional drag terms, as defined by Nikora et al. (2019), are

$$F_{3D} = \int_{z_b}^{z_s} (z_s - z)^2 \left(\frac{\partial \phi \langle \bar{p} \rangle}{\partial x} - \frac{1}{h} \int_{z_b}^{z_s} \frac{\partial \phi \langle \bar{p} \rangle}{\partial x} dz \right) dz \quad (\text{B1})$$

$$+ \int_{z_b}^{z_s} (z_s - z)^2 \left(\rho \phi \left(\frac{\partial \langle \bar{u} \rangle}{\partial t} + \langle \bar{v} \rangle \cdot \nabla \langle \bar{u} \rangle \right) - \frac{1}{h} \int_{z_b}^{z_s} \rho \phi \left(\frac{\partial \langle \bar{u} \rangle}{\partial t} + \langle \bar{v} \rangle \cdot \nabla \langle \bar{u} \rangle \right) dz \right) dz \quad (\text{B2})$$

$$+ \int_{z_b}^{z_s} (z_s - z)^2 \left[\frac{\partial}{\partial x} \left\langle \mu \frac{\partial \bar{u}}{\partial x} \right\rangle_s + \frac{\partial}{\partial x} \left\langle \mu \frac{\partial \bar{v}}{\partial y} \right\rangle_s + \frac{\partial \phi \langle \bar{\tau}_{xx} \rangle}{\partial x} + \frac{\partial \phi \langle \bar{\tau}_{xy} \rangle}{\partial y} \right] dz \quad (\text{B3})$$

$$- \frac{1}{h} \int_{z_b}^{z_s} \left(\frac{\partial}{\partial x} \left\langle \mu \frac{\partial \bar{u}}{\partial x} \right\rangle_s + \frac{\partial}{\partial x} \left\langle \mu \frac{\partial \bar{v}}{\partial y} \right\rangle_s + \frac{\partial \phi \langle \bar{\tau}_{xx} \rangle}{\partial x} + \frac{\partial \phi \langle \bar{\tau}_{xy} \rangle}{\partial y} \right) dz \quad (\text{B4})$$

where the first term describes the deviations from depth-averaged pressure force, the second term describes the deviations from depth-averaged inertial forces, and the third term describes the deviations from depth-averaged fluid forces (Nikora et al., 2019).

The prefactor is

$$N_o = \frac{1}{2} \left(\frac{3}{h^2 \phi \langle \bar{\tau}_o \rangle} \int_{z_b}^{z_k} (z_s - z)^2 \phi \langle \bar{f}_d \rangle dz + \frac{3}{h^3} \int_{z_b}^{z_s} (z_s - z)^2 (1 - \phi) dz - \left(\frac{z_s - z_b}{h} \right)^3 \right) \quad (\text{B5})$$

where the first term is a drag length-scale (Nikora et al., 2019) and the second term is a roughness-depth length-scale (Nikora et al., 2019). It reduces to $N_o = 1$ for simple 2D deep flows.

Appendix C: Frontal and Planform Solidity

The total upstream-facing area A_f and planform area A_p of a representative channel cross-section with N boulders can be written as follows:

$$A_f = \sum_i^N A_{fi} = N \langle A_{fi} \rangle; \quad A_p = \sum_i^N A_{pi} = N \langle A_{pi} \rangle \quad (\text{C1})$$

where A_{fi} and A_{pi} are the upstream-facing and planform area of the i th boulder and $\langle A_{fi} \rangle$ and $\langle A_{pi} \rangle$ are the average upstream-facing and planform area of the boulders in a reach. The average planform area of a boulder is

$$\langle A_{pi} \rangle = s_1 k_s^2 \quad (\text{C2})$$

where s_1 is a shape factor relating the planform area of a boulder to the roughness length-scale, k_s . The average number of boulders, N , can be related to the planform boulder density, also known as the planform solidity λ_p (Chung et al., 2021)

$$\lambda_p = \frac{A_p}{A_o} = \frac{s_1 k_s^2}{\lambda^2} = \frac{N s_1 k_s^2}{A_o} \quad (\text{C3})$$

where λ is the average spacing between boulders and $A_o = W k_s$ is the planform area of the channel boundary associated with a channel cross-section.

The average upstream-facing area of a single roughness element should scale with $\sim k_s^2$ or $\sim k_s H$, or something in-between, depending on the flow depth and the shape of the boulders. This can be written as follows:

$$\langle A_{fi} \rangle = s_2 k_s^2 (H/k_s)^{1-a} \quad (C4)$$

where $0 \leq a \leq 1$ and s_2 is a shape factor relating the drag area of the average element to the length-scale k_s . Therefore the frontal solidity is

$$\lambda_f = \frac{A_f}{A_o} = \frac{A_p}{A_o} \frac{A_f}{A_p} = s \lambda_p \left(\frac{H}{\gamma D_{84}} \right)^{1-a} \quad (C5)$$

where the shape factors have been combined into $s = s_2/s_1$. Finally the upstream-facing boulder area per unit channel cross-sectional area is

$$\frac{A_f}{A_c} = \frac{A_f}{A_o} \frac{A_o}{A_c} = s \lambda_p \left(\frac{H}{\gamma D_{84}} \right)^{1-a} \frac{W k_s}{W H} = s \lambda_p \left(\frac{H}{\gamma D_{84}} \right)^{-a} \quad (C6)$$

List of Notation

ρ	density of water
g	acceleration due to gravity
$S = \cos \theta$	downstream channel slope
$\cos \varphi$	lateral channel slope (toward channel centerline)
μ, ν	dynamic and kinematic viscosity of water
κ	von Kármán constant
u, v, w	instantaneous flow velocity in the $x, y,$ and z direction, respectively
$\bar{\cdot}, \langle \cdot \rangle, \langle \bar{\cdot} \rangle, \langle \bar{\cdot} \rangle$	symbols to denote time average, spatial average, double-average, and depth- and double-averaged, respectively
$u, \langle \bar{u} \rangle, \langle \bar{u} \rangle, U$	instantaneous, double-averaged, double- and depth-averaged (local-scale), and double-, depth-, and width averaged flow velocity (channel-scale)
z_b, z_s, z_k	lowest and highest fluid-occupied elevation, and highest elevation of roughness boundary layer in a downstream x - z slice of channel, respectively
k_s	equivalent sand grain roughness
B_s	equivalent sand grain roughness correction to logarithmic law of the wall
D_{84}	grain size of 84th percentile in a channel
$\gamma = k_s/D_{84} \approx 3.5$	ratio of equivalent sand grain roughness to grain size of 84th percentile
h, H	averaged flow depth, local- and channel-scale, respectively
W	average channel width at the surface
$A_c = HW$	double-averaged channel cross-sectional area
$Q = HUW$	channel water flux
P_c	double-average channel perimeter
$R = A_c/P_c$	hydraulic radius
$R_v = H = A_c/W \geq R$	volumetric hydraulic radius
L	downstream length of double-averaging volume
V_o	volume of double-averaging region
V_f	volume of double-averaging region occupied by fluid
$\phi = V_f/V_o$	average porosity (fraction of double-averaging volume occupied by fluid normalized by total volume)
$A_o = P_c k_s$	planform area of average channel cross-section
$\langle f_v \rangle, \langle \bar{f}_v \rangle$	viscous drag force per unit volume at different scales
$\langle \bar{f}_p \rangle, \langle \bar{f}_p \rangle, F_p$	pressure drag force per unit volume at different scales
$\langle \bar{f}_d \rangle, \langle \bar{f}_d \rangle$	total drag force per unit volume at different scales
$\langle \bar{\tau}_o \rangle, \tau_o$	local- and channel-scale boundary shear stress
$\langle \bar{u}_* \rangle, u_* = \sqrt{\tau_o/\rho}$	local- and channel-scale shear velocity
$\langle \bar{C}_f \rangle, C_f = 2\tau_o/\rho U^2$	local- and channel-scale coefficients of drag

C_D	coefficient of form drag on a single grain
U_p	flow velocity averaged over all roughness elements in reach
c_1	coefficient relating U_p to channel-scale average flow velocity U
r	exponent of power-law flow resistance model for rough boundaries
a	exponent controlling rate of change in upstream-facing boulder area, A_p , with relative flow depth, H/D_{84}
\bar{p}	time averaged pressure on roughness elements
N	average number of roughness elements in channel cross-section
λ	average spacing of large roughness elements
$A_{\bar{p}i}, \langle A_{\bar{p}i} \rangle$	upstream-facing area of i th roughness element and average upstream-facing area of roughness element
$A_f = \sum_i^N A_{fi} = N A_{fi}$	total upstream area of roughness elements in channel cross-section
$A_{pi}, \langle A_{pi} \rangle$	planform area of i th roughness element and average planform area of roughness element
$A_p = \sum_i^N A_{pi} = N A_{pi}$	total planform area of roughness elements in channel cross-section
$s_1 = \langle A_{pi} \rangle / k_s^2$	shape factor relating average planform area of large roughness elements to equivalent sand grain roughness
$s_2 = \langle A_{fi} \rangle / k_s^{1+a}$	shape factor relating average upstream-facing area of large roughness elements to equivalent sand grain roughness
$s = s_2 / s_1$	combined shape factors
λ_p	fraction of planform channel area occupied by boulders per unit channel planform area, a measure of boulder density
λ_f	fraction of cross-sectional channel area occupied by boulders per unit channel planform area, a measure of boulder density

Data Availability Statement

All data used in this work are available at <http://www.hydroshare.org/resource/0629ffb81fdb40aa9e6be42cc11918ca>

References

- Aberle, J., & Nikora, V. (2006). Statistical properties of armored gravel bed surfaces. *Water Resources Research*, 42(11), W11414. <https://doi.org/10.1029/2005wr004674>
- Bathurst, J. C. (1985). Flow resistance estimation in mountain rivers. *Journal of Hydraulic Engineering*, 111(4), 625–643. [https://doi.org/10.1061/\(asce\)0733-9429\(1985\)111:4\(625\)](https://doi.org/10.1061/(asce)0733-9429(1985)111:4(625))
- Brereton, G., Jouybari, M. A., & Yuan, J. (2021). Toward modeling of turbulent flow over surfaces of arbitrary roughness. *Physics of Fluids*, 33(6), 065121. <https://doi.org/10.1063/5.0051097>
- Carling, P. A., Hoffmann, M., Silke-Blatter, A., & Dittrich, A. (2002). Drag of emergent and submerged rectangular obstacles in turbulent flow above bedrock surface. In A. J. Schleiss, & E. Bollaert (Eds.), *[Papers in proceedings of] International workshop on "Rock Scour"* (pp. 83–94). Chan, L., MacDonald, M., Chung, D., Hutchins, N., & Ooi, A. (2015). A systematic investigation of roughness height and wavelength in turbulent pipe flow in the transitionally rough regime. *Journal of Fluid Mechanics*, 771, 743–777. <https://doi.org/10.1017/jfm.2015.172>
- Chauvet, H., Devauchelle, O., Métivier, F., Lajeunesse, E., & Limare, A. (2014). Recirculation cells in a wide channel. *Physics of Fluids*, 26(1), 016604. <https://doi.org/10.1063/1.4862442>
- Cheng, N.-S. (2017). Simple modification of Manning-Strickler formula for large-scale roughness. *Journal of Hydraulic Engineering*, 143(9), 04017031. [https://doi.org/10.1061/\(asce\)hy.1943-7900.0001345](https://doi.org/10.1061/(asce)hy.1943-7900.0001345)
- Chung, D., Hutchins, N., Schultz, M. P., & Flack, K. A. (2021). Predicting the drag of rough surfaces. *Annual Review of Fluid Mechanics*, 53(1), 439–471. <https://doi.org/10.1146/annurev-fluid-062520-115127>
- Cox, B. L., & Wang, J. (1993). Fractal surfaces: Measurement and applications in the Earth sciences. *Fractals*, 1(01), 87–115. <https://doi.org/10.1142/s0218348x93000125>
- Deal, E. (2021). Downstream hydraulic geometry data compilation. Retrieved from <http://www.hydroshare.org/resource/0629ffb81fdb40aa9e6be42cc11918ca>
- Dey, S., & Das, R. (2012). Gravel-bed hydrodynamics: Double-averaging approach. *Journal of Hydraulic Engineering*, 138(8), 707–725. [https://doi.org/10.1061/\(asce\)hy.1943-7900.0000554](https://doi.org/10.1061/(asce)hy.1943-7900.0000554)
- Ferguson, R. (1986). Hydraulics and hydraulic geometry. *Progress in Physical Geography*, 10(1), 1–31. <https://doi.org/10.1177/030913338601000101>
- Ferguson, R. (2007). Flow resistance equations for gravel- and boulder-bed streams. *Water Resources Research*, 43(5), W05427. <https://doi.org/10.1029/2006wr005422>
- Flack, K. A., & Schultz, M. P. (2014). Roughness effects on wall-bounded turbulent flows. *Physics of Fluids*, 26(10), 101305. <https://doi.org/10.1063/1.4896280>
- Fukagata, K., Iwamoto, K., & Kasagi, N. (2002). Contribution of Reynolds stress distribution to the skin friction in wall-bounded flows. *Physics of Fluids*, 14(11), L73–L76. <https://doi.org/10.1063/1.1516779>

Acknowledgments

I would like to thank Dr. Ellen Wohl, Dr. Dieter Rickenmann, Dr. Thomas Ashley and one anonymous reviewer for their time as well as their insightful and helpful comments on this work. In addition, I thank Dr. Jens Turowski and Dr. Ron Nativ for interesting discussions on the topic of flow resistance in boulder-mantled channels that helped me formulate some of ideas discussed in this paper.

- Giménez-Curto, L. A., & Lera, M. A. C. (1996). Oscillating turbulent flow over very rough surfaces. *Journal of Geophysical Research*, *101*(C9), 20745–20758. <https://doi.org/10.1029/96jc01824>
- Hey, R. D. (1979). Flow resistance in gravel-bed rivers. *Journal of the Hydraulics Division*, *105*(4), 365–379. <https://doi.org/10.1061/jyceaj.0005178>
- Kalathil, S. T., & Chandra, V. (2019). Review of step-pool hydrodynamics in mountain streams. *Progress in Physical Geography: Earth and Environment*, *43*(5), 607–626. <https://doi.org/10.1177/0309133319859807>
- Keulegan, G. H. (1938). *Laws of turbulent flow in open channels* (Vol. 21). National Bureau of Standards.
- King, J. G. (2004). *Sediment transport data and related information for selected coarse-bed streams and rivers in Idaho (No. 131)*. US Department of Agriculture, Forest Service, Rocky Mountain Research Station.
- Knight, D. (1996). River channel and floodplain hydraulics. *Chapter 5. Floodplain processes* (pp. 139–181). John Wiley and Sons Ltd.
- Kuwata, Y., & Kawaguchi, Y. (2019). Direct numerical simulation of turbulence over systematically varied irregular rough surfaces. *Journal of Fluid Mechanics*, *862*, 781–815. <https://doi.org/10.1017/jfm.2018.953>
- Lamb, M. P., Brun, F., & Fuller, B. M. (2017a). Direct measurements of lift and drag on shallowly submerged cobbles in steep streams: Implications for flow resistance and sediment transport. *Water Resources Research*, *53*(9), 7607–7629. <https://doi.org/10.1002/2017wr020883>
- Lamb, M. P., Brun, F., & Fuller, B. M. (2017b). Hydrodynamics of steep streams with planar coarse-grained beds: Turbulence, flow resistance, and implications for sediment transport. *Water Resources Research*, *53*(3), 2240–2263. <https://doi.org/10.1002/2016wr019579>
- Lawrence, D. (2000). Hydraulic resistance in overland flow during partial and marginal surface inundation: Experimental observations and modeling. *Water Resources Research*, *36*(8), 2381–2393. <https://doi.org/10.1029/2000wr900095>
- Lepp, L., Koger, C. J., & Wheeler, J. A. (1993). Channel erosion in steep gradient, gravel-paved streams. *Bulletin of the Association of Engineering Geologists*, *30*(4), 443–454. <https://doi.org/10.2113/gseegeosci.xxx.4.443>
- Luo, M., Ye, C., Wang, X., Huang, E., & Yan, X. (2022). Analytical model of flow velocity in gravel-bed streams under the effect of gravel array with different densities. *Journal of Hydrology*, *608*, 127581. <https://doi.org/10.1016/j.jhydrol.2022.127581>
- MacDonald, M., Ooi, A., García-Mayoral, R., Hutchins, N., & Chung, D. (2018). Direct numerical simulation of high aspect ratio spanwise-aligned bars. *Journal of Fluid Mechanics*, *843*, 126–155. <https://doi.org/10.1017/jfm.2018.150>
- Morvan, H., Knight, D., Wright, N., Tang, X., & Crossley, A. (2008). The concept of roughness in fluvial hydraulics and its formulation in 1d, 2d and 3d numerical simulation models. *Journal of Hydraulic Research*, *46*(2), 191–208. <https://doi.org/10.1080/00221686.2008.9521855>
- Nikora, V., Ballio, F., Coleman, S., & Pokrajac, D. (2013). Spatially averaged flows over mobile rough beds: Definitions, averaging theorems, and conservation equations. *Journal of Hydraulic Engineering*, *139*(8), 803–811. [https://doi.org/10.1061/\(asce\)hy.1943-7900.0000738](https://doi.org/10.1061/(asce)hy.1943-7900.0000738)
- Nikora, V., Goring, D., McEwan, I., & Griffiths, G. (2001). Spatially averaged open-channel flow over rough bed. *Journal of Hydraulic Engineering*, *127*(2), 123–133. [https://doi.org/10.1061/\(asce\)0733-9429\(2001\)127:2\(123\)](https://doi.org/10.1061/(asce)0733-9429(2001)127:2(123))
- Nikora, V., Koll, K., McEwan, I., McLean, S., & Dittrich, A. (2004). Velocity distribution in the roughness layer of rough-bed flows. *Journal of Hydraulic Engineering*, *130*(10), 1036–1042. [https://doi.org/10.1061/\(asce\)0733-9429\(2004\)130:10\(1036\)](https://doi.org/10.1061/(asce)0733-9429(2004)130:10(1036))
- Nikora, V., McEwan, I., McLean, S., Coleman, S., Pokrajac, D., & Walters, R. (2007). Double-averaging concept for rough-bed open-channel and overland flows: Theoretical background. *Journal of Hydraulic Engineering*, *133*(8), 873–883. [https://doi.org/10.1061/\(asce\)0733-9429\(2007\)133:8\(873\)](https://doi.org/10.1061/(asce)0733-9429(2007)133:8(873))
- Nikora, V., Stoesser, T., Cameron, S. M., Stewart, M., Papadopoulos, K., Ouro, P., et al. (2019). Friction factor decomposition for rough-wall flows: Theoretical background and application to open-channel flows. *Journal of Fluid Mechanics*, *872*, 626–664. <https://doi.org/10.1017/jfm.2019.344>
- Nitsche, M., Rickenmann, D., Kirchner, J. W., Turowski, J., & Badoux, A. (2012). Macroroughness and variations in reach-averaged flow resistance in steep mountain streams. *Water Resources Research*, *48*(12). <https://doi.org/10.1029/2012wr012091>
- Papanicolaou, A., & Tsakiris, A. G. (2017). Boulder effects on turbulence and bedload transport. *Gravel-Bed Rivers*, 33–72. <https://doi.org/10.1002/9781118971437.ch2>
- Powell, D. M. (2014). Flow resistance in gravel-bed rivers: Progress in research. *Earth-Science Reviews*, *136*, 301–338. <https://doi.org/10.1016/j.earscirev.2014.06.001>
- Power, W. L., & Tullis, T. E. (1991). Euclidean and fractal models for the description of rock surface roughness. *Journal of Geophysical Research*, *96*(B1), 415–424. <https://doi.org/10.1029/90jb02107>
- Raupach, M. R., & Shaw, R. (1982). Averaging procedures for flow within vegetation canopies. *Boundary-Layer Meteorology*, *22*(1), 79–90. <https://doi.org/10.1007/bf00128057>
- Rickenmann, D., & Recking, A. (2011). Evaluation of flow resistance in gravel-bed rivers through a large field data set. *Water Resources Research*, *47*(7). <https://doi.org/10.1029/2010wr009793>
- Sarkar, S., & Dey, S. (2010). Double-averaging turbulence characteristics in flows over a gravel bed. *Journal of Hydraulic Research*, *48*(6), 801–809. <https://doi.org/10.1080/00221686.2010.526764>
- Schlichting, H., & Gersten, K. (2015). *Boundary layer theory*. Springer.
- Schneider, J. M., Rickenmann, D., Turowski, J. M., & Kirchner, J. W. (2015). Self-adjustment of stream bed roughness and flow velocity in a steep mountain channel. *Water Resources Research*, *51*(10), 7838–7859. <https://doi.org/10.1002/2015wr016934>
- Shobe, C. M., Turowski, J. M., Nativ, R., Glade, R. C., Bennett, G. L., & Dini, B. (2021). The role of infrequently mobile boulders in modulating landscape evolution and geomorphic hazards. *Earth-Science Reviews*, *220*, 103717. <https://doi.org/10.1016/j.earscirev.2021.103717>
- Smart, G. M., Duncan, M. J., & Walsh, J. M. (2002). Relatively rough flow resistance equations. *Journal of Hydraulic Engineering*, *128*(6), 568–578. [https://doi.org/10.1061/\(asce\)0733-9429\(2002\)128:6\(568\)](https://doi.org/10.1061/(asce)0733-9429(2002)128:6(568))
- Stewart, M. T., Cameron, S. M., Nikora, V. I., Zampiron, A., & Marusic, I. (2019). Hydraulic resistance in open-channel flows over self-affine rough beds. *Journal of Hydraulic Research*, *57*(2), 183–196. <https://doi.org/10.1080/00221686.2018.1473296>
- Whitaker, S. (1986). Flow in porous media i: A theoretical derivation of Darcy's law. *Transport in Porous Media*, *1*(1), 3–25. <https://doi.org/10.1007/bf01036523>
- Williams, G. P., & Rosgen, D. L. (1989). *Measured total sediment loads (suspended loads and bedloads) for 93 United States streams*. US Geological Survey Washington.
- Wilson, N. R., & Shaw, R. H. (1977). A higher order closure model for canopy flow. *Journal of Applied Meteorology (1962-1982)*, *16*(11), 1197–1205. [https://doi.org/10.1175/1520-0450\(1977\)016<1197:ahocmf>2.0.co;2](https://doi.org/10.1175/1520-0450(1977)016<1197:ahocmf>2.0.co;2)
- Xu, F., Coco, G., Zhou, Z., Townend, I., Guo, L., & He, Q. (2020). A universal form of power law relationships for river and stream channels. *Geophysical Research Letters*, *47*(20), e2020GL090493. <https://doi.org/10.1029/2020gl090493>